Advances in Water Resources 113 (2018) 180–188

Contents lists available at ScienceDirect

Advances in Water Resources

journal homepage: www.elsevier.com/locate/advwatres

Anomalous behaviors during infiltration into heterogeneous porous media

F.D.A. Aarão Reis[a], D. Bolster[b], V.R. Voller[*,c]

[a] Instituto de Física, Universidade Federal Fluminense, Avenida Litorânea s/n, Niterói, RJ 24210-340, Brazil
[b] Department of Civil & Environmental Engineering and Earth Sciences, University of Notre Dame. South Bend, USA
[c] Department of Civil, Environmental, and Geo- Engineering, University of Minnesota, Minneapolis, USA

ARTICLE INFO

Keywords:
Anomalous transport
Infiltration
Fractal dimension

ABSTRACT

Flow and transport in heterogeneous porous media often exhibit anomalous behavior. A physical analog example is the uni-directional infiltration of a viscous liquid into a horizontal oriented Hele-Shaw cell containing through thickness flow obstacles; a system designed to mimic a gravel/sand medium with impervious inclusions. When there are no obstacles present or the obstacles form a multi-repeating pattern, the change of the length of infiltration F with time t tends to follow a Fickian like scaling, $F \sim t^{\frac{1}{2}}$. In the presence of obstacle fields laid out as Sierpinski carpet fractals, infiltration is anomalous, i.e., $F \sim t^n$, $n \neq 1/2$. Here, we study infiltration into such Hele-Shaw cells. First we investigate infiltration into a square cell containing one fractal carpet and make the observation that it is possible to generate both sub ($n < 1/2$) and super ($n > 1/2$) diffusive behaviors within identical heterogeneity configurations. We show that this can be explained in terms of a scaling analysis developed from results of random-walk simulations in fractal obstacles; a result indicating that the nature of the domain boundary controls the exponent n of the resulting anomalous transport. Further, we investigate infiltration into a rectangular cell containing several repeats of a given Sierpinski carpet. At very early times, before the liquid encounters any obstacles, the infiltration is Fickian. When the liquid encounters the first (smallest scale) obstacle the infiltration sharply transitions to sub-diffusive. Subsequently, around the time where the liquid has sampled all of the heterogeneity length scales in the system, there is a rapid transition back to Fickian behavior. An explanation for this second transition is obtained by developing a simplified infiltration model based on the definition of a representative *averaged* hydraulic conductivity.

1. Introduction

The term anomalous transport typically refers to transport processes where the scale of spreading of a substance does not scale in time in a manner consistent with a Fickian description. The prototypical example, so called *anomalous diffusion*, is where the classical time exponent of $n = \frac{1}{2}$, associated with the spreading length scale of a diffusing plume ($\ell \sim t^n$), is replaced by super- ($n > \frac{1}{2}$) or sub- ($n < \frac{1}{2}$) diffusion exponent. Although the name might suggest otherwise, anomalous transport occurs in and across so many systems that some have suggested it should be called ubiquitous transport (Eliazar and Klafter, 2011). Physical systems that display characteristics of anomalous transport are abundant and within the context of water resources include flow and transport in porous media (Benson et al., 2001; De Anna et al., 2013; Edery et al., 2014; Le Borgne et al., 2008), streams and rivers (Aubeneau et al., 2014; 2015; Gooseff et al., 2005; Haggerty et al., 2002), fractured media (Berkowitz and Scher, 1997; Kang et al., 2016; Wang and Cardenas, 2014), turbulent flows (Cushman-Roisin, 2008), biofilms (Seymour et al., 2004), sediment transport (Foufoula-Georgiou et al., 2010; Ganti et al., 2010; González et al., 2017), and surficial earth processes (Falcini et al., 2013; Finnegan et al., 2014; Schumer et al., 2009; Stark et al., 2009; Voller et al., 2012; Voller and Paola, 2010). The origins of anomalous transport are not unique and causes can be difficult to disentangle (e.g. Dentz and Bolster, 2010), but the emergence of anomalous behaviors is typically characterized by the presence of broad scale heterogeneities, occurring over multiple scales, as is often seen in natural porous media (Berkowitz et al., 2006; Bijeljic and Blunt, 2006; Dentz et al., 2004; Gouze et al., 2008; Kang et al., 2014; Le Borgne and Gouze, 2008; Neuman and Tartakovsky, 2009; Serrano, 1997; Voller, 2011), where the heterogeneity, ranging from grain sizes of millimeters to geological inclusions of km, promote the appearance of *fast paths* as well as regions of *hold up*.

While anomalous transport has been observed time and time again in natural systems, a general open question still remains as how to link physical characteristics of the heterogeneous medium to measurable quantities associated with anomalous transport such as the time

* Corresponding author.
E-mail address: volle001@umn.edu (V.R. Voller).

https://doi.org/10.1016/j.advwatres.2018.01.010
Received 17 October 2017; Received in revised form 9 January 2018; Accepted 10 January 2018
Available online 11 January 2018
0309-1708/

exponent n. With a view to addressing this, Voller and co-workers (Filipovitch et al., 2016; Voller, 2015) used numerical and physical experiments to track the infiltration of liquid into a horizontally oriented Hele-Shaw cell, i.e., a two-dimensional potential flow domain established between two closely spaced plates. In their setup, the cell had a square plan view $\ell \times \ell$ and the combination of the plate spacing and the viscosity of the infiltrating fluid were chosen in such a way that the measured and simulated infiltration could be considered to be equivalent to Darcy flow into a sand/gravel medium (Batchelor, 1967). The role of the control of heterogeneity on the nature of the infiltration was investigated and three general configurations were considered (i) empty cells with no flow obstacles, (ii) flow obstacles forming, in plan view, a repeating pattern, and (iii) flow obstacles forming, in plan view, a truncated fractal pattern (Serpinski carpet). In each test cell, a directional flow into the initially empty (gas filled) cavity was driven by a fixed head, applied along the inlet edge at $x = 0$. The progress of infiltration into the cell was measured as

$$F(t) = \frac{\text{Plan-view Area of Invading Liquid}}{\ell}, \tag{1}$$

referred to as the *length of infiltration*.

In both experiments and simulations, for cases (i) and (ii), when no obstacles were present or when obstacles formed a repeating pattern, the length of infiltration tended to a Fickian diffusion like signal, i.e.,

$$F = at^n, \quad n = \frac{1}{2} \tag{2}$$

where a is a constant (Filipovitch et al., 2016; Voller, 2015). When the obstacles formed a truncated Sierpinski carpet, a power law scaling was still observed but the exponent was sub-diffusive, i.e., $n < \frac{1}{2}$. Further, the agreement between the experimental measurements and the numerical simulation predictions is within 95% confidence limits, a result that suggests the physical validity of the simulation.

The observations of the nature of infiltration into a fractal obstacle field has also been related to the fundamental physics of diffusion processes. The governing equations used in the direct continuum simulations of infiltration into Hele-Shaw cells (Voller, 2015) have the form of a diffusion transport process, i.e., they are controlled by the divergence of a potential gradient. In simple settings, e.g., the spreading of an initial pulse, it is well known that we can directly relate diffusion transport to the tracking of the random (Brownian) motion of particles on a lattice (Einstein, 1905). Starting from this point, Aarão Reis (2016) constructed a simulation for the infiltration of random walkers, from a common boundary with continuos refreshment, into a Sierpinski carpet. Observations of the change of infiltration length with time (determined from the sum of lattice sites occupied by particles) showed anomalous sub-diffusive exponents n consistent with the experiments and continuum simulations of infiltration into obstacle filled Hele-Shaw cells (Filipovitch et al., 2016; Voller, 2015). Further, through accounting for the dimensions of the bulk fractal and of the boundary from which the walkers entered the carpet, Aarão Reis (2016) established a scaling that related the infiltration exponent n to the well known sub-diffusive time exponent $\nu < \frac{1}{2}$ characterizing the spreading of free walkers starting from a common point within a fractal obstacle field (Havlin and Ben-Avraham, 2002; Kim et al., 1993; Reis, 1995).

In the study of infiltration into obstacle fields open questions with important practical implications remain. First, while anomalous behaviours has been reported in the literature there is ambiguity as to its exact nature. For example, in fitting a fractional Richards model to data of moisture migration into brick, Gerolymatou et al. (2006) arrive at a sub-diffusive infiltration time exponent of $n = 0.43$, in line with values reported by Voller (2015) and Filipovitch et al. (2016). On the other hand, in another experimental study of moisture infiltration into brick, Küntz and Lavallée (2001) report a super-diffusive time exponent of $n = 0.58$. This begs the question: *How might it be possible for essentially the same heterogeneous system to exhibit both sub- and super- dispersive infiltration behaviors?*

Further, we note that the Hele-Shaw experimental and simulation observations were all made over the time scale of the complete infiltration into a unit fractal obstacle field. In the context of solute transport through a heterogeneous system, however, we would expect, depending on the time and spacial scales, to see transitions between normal and anomalous behaviors (e.g. Bolster et al., 2011; Dentz et al., 2004; Sund et al., 2016; Taylor, 1954; Whitaker, 2013). At early times, before the solute encounters any heterogeneity (obstacles), the transport is Fickian. Anomalous transport occurs at intermediate time scales where the solute is navigating through heterogeneities with ever changing length scales. Once the solute samples all heterogeneity in the system, normal transport is resumed. Thus we ask: *Are such transport transitions observed in our Hele-Shaw infiltration simulations and if so, once the largest obstacle (heterogeneity) length scale has been sampled by the infiltrating liquid, how long does it take for the infiltration to return to a normal diffusive scaling?*

The core objectives of this work are to identify the conditions under which both sub- and super- diffusive behaviors can be induced by the exact same heterogeneous system and to examine the nature of transitions between normal and anomalous behavior. Towards this end we begin by revisiting the main results in the recent work on infiltration into a Hele-Shaw cell containing flow obstacles (Filipovitch et al., 2016; Voller, 2015). We make two new departures from this starting point. In the first instance, we demonstrate that the observed sub-diffusive behaviors seen in these direct continuum simulations match the scaling reported for random walk simulations (Aarão Reis, 2016). This allows us to induce *super*-diffusive infiltration behaviors in our simulations, by simply relocating the boundary over which the liquid is introduced into the Hele-Shaw cell. In our second departure, we investigate diffusion behavior transitions during the infiltration into an obstacle field made up of a repeating pattern of unit Sierpinski carpets. We note two transitions, at early time, from normal to sub- and then, at later time, from sub- back to normal. Emphasis is placed on identifying the location and scale over which the second of these transitions occurs.

2. Sub-diffusive and normal diffusive behavior

We start by summarizing key results for infiltration in the fractal carpets reported in Voller (2015) and Filipovitch et al. (2016). We consider the three plan-form carpet designs shown in Fig. 1. These are 2nd order Sierpinski 1×1 carpets of pattern numbers (a) $N = 3$ and (b)

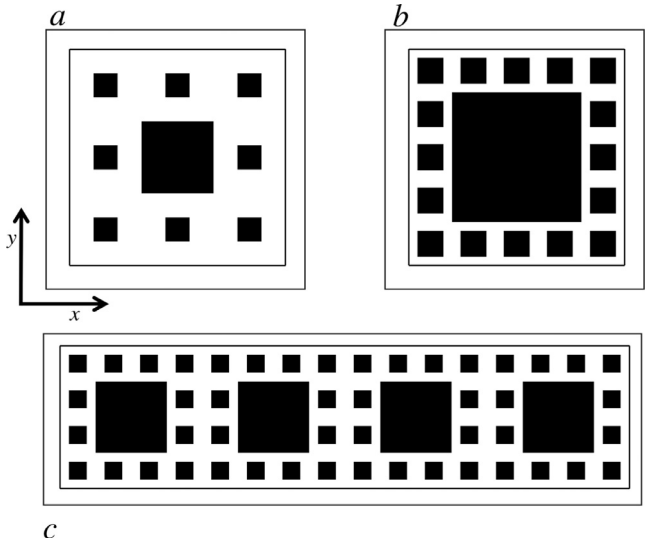

Fig. 1. Obstacle carpet patterns. *a.* 1×1, $N = 3$, 2nd order Sierpinski, *b.* 1×1, $N = 5$, 2nd order Sierpinski, *c.* Horizontal four-fold repeat of a 1×1, $N = 4$, 2nd order Sierpinski.

$N = 5$ as well as (c) a carpet of size 4×1 made up of a four fold repeat of a 2nd order 1×1 Sierpinski carpet with pattern number $N = 4$. The carpet spaces are initially empty (gas filled) and liquid is infiltrated along the left-hand side by imposing a fixed unit pressure head along the boundary $x = 0$. The pressure head on the liquid/gas front within the carpet is set zero. Voller (2015) developed a Volume of Fluid (Hirt and Nichols, 1981) method to track the infiltration, which we use here, drawing on extensively verified and validated codes (Bruschke and Advani, 1990; Voller and Chen, 1996). In these simulations, in the spaces between obstacles, we set the fluidic conductivity as $K_{space} = 1$, within obstacles we set the conductivity to an arbitrarily small value, e.g., $K_{obs} = 10^{-15}$. For the $N = 3$ and $N = 5$ carpets, the numerical calculations use a fixed time step value of $\Delta t = 0.01$ and space steps $\Delta x = \Delta y = \frac{1}{2N^2}$; values that provide grid independent results. Simulations are terminated when the first infiltrating liquid arrives in the last column of cells in the computational domain. Some further information on the numerics are provided in an appendix; details of the full numerical implementation, testing, and verification is detailed in Voller (2015) and experimental validation can be found in Filipovitch et al. (2016).

Fig. 2 reports, as red-circles, the simulated log-log plot of length of infiltration F vs. time t for the $N = 3$ and $N = 5$ single carpets. As previously observed by Voller (2015), the black lines provide sound fits to the simulated measurements. Note, however, due to the fact that the local conditions (distribution of space and obstacle) undergo abrupt changes each time the infiltrating fluid encounters a new line of obstacles, we should not expect the infiltration predictions to be smooth, i.e., there will be slope changes in the log-log plot. These log-periodic oscillations are characteristic of kinetic models in deterministic fractals (Akkermans et al., 2008; Bab et al., 2008a; 2008b) and were recently observed in simulations of random walker infiltration from a boundary in high order carpet patterns (Aarão Reis, 2016). Nevertheless, the overall infiltration predictions in Fig. 2 show a strong linear trend, well characterized by a single sub-diffusive time exponent $n < 1/2$. In the original work by Voller (2015) the exponents n were obtained by a least squares fit. Here, by contrast, we make the *ansatz* that the scaling relating the time exponent of random walk infiltration from a boundary to random walkers from a point within the obstacle domain, identified by Aarão Reis (2016), can also be used for our continuum simulations (see details in Appendix). That is we determine the time exponent from

Table 1
Properties of fractal carpets and calculated power-law coefficients a and exponents n. Estimates of ν are from (Kim et al., 1993; Reis, 1995).

Pattern	D_F, Eq. (4)	D_B, Eq. (5)	ν	a, Eq. (2)	n, Eq. (3)
$N = 3$	1.89279	1	0.475	0.917	0.424
$N = 4$	1.79248	1	0.462	0.592	0.366
$N = 5$	1.72271	1	0.455	0.385	0.329
$N_{shift} = 3$	1.89279	0.63093	0.475	1.010	0.599
$N_{shift} = 5$	1.72271	0.43067	0.455	0.407	0.588

$$n = \nu(D_F - D_B) \tag{3}$$

where

$$D_F = \frac{\log(4N - 4)}{\log(N)} \tag{4}$$

is the fractal dimension of the carpet obstacle pattern, D_B is the fractal dimension of the boundary over which the liquid enters, and $\nu < \frac{1}{2}$ is the sub-diffusive time exponent of the spreading of random walkers within the carpet. The appropriate values for our carpets are given in the Table 1. For the power-law fits in Fig. 2, the boundary over which the liquid enters is free of any obstacles so its fractal dimension is $D_B = 1$ and the values ν given in Table 1 are those previously calculated from random walk simulations starting from a common point within the appropriate Carpets (Balankin, 2017; Kim et al., 1993; Reis, 1995). Thus, we stress that the exponent values, obtained from Eq. (3) and listed in the last column of Table 1, are independent of those observed in our simulations. The only tie to simulation data is setting the coefficient a in the power-law, Eq. (2) (see penultimate column in Table 1) obtained by forcing the power-law fit to pass through the terminal simulation values of F and t. The infiltration simulation into the four-fold repeated 2nd order $N = 4$ (using $\Delta t = 0.01$, $\Delta x = \Delta y = \frac{1}{N^2}$) Fig. 3, tells a slightly different story. Due to the fact that, in the left hand panel of the figure, a power-law with exponent $n = \frac{1}{2}$ provides a close fit to the simulation, it appears that the F vs. t data confirms the assertion, made by Voller (2015), that when the obstacle pattern is repeated the infiltration exhibits normal diffusive behavior. Inspection of the log-log plot (in the right panel) however, reveals a more subtle picture. In particular, at earlier times, the advance of infiltration appears to be sub-diffusive and well characterized by the time exponent $n = 0.366$ determined by the

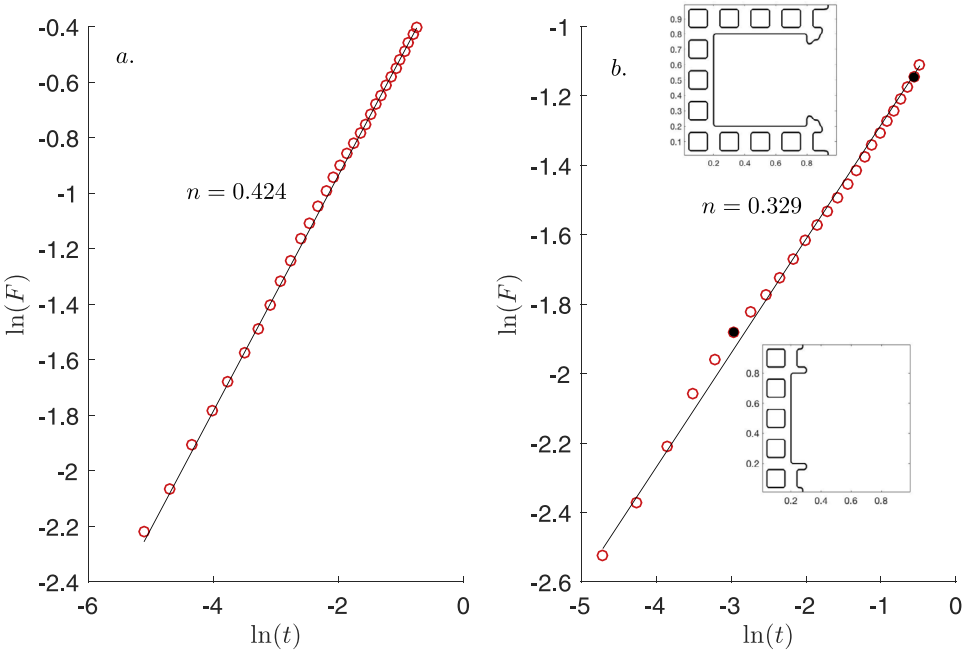

Fig. 2. Log-log plots (red-circles) of calculated infiltration $F(t)$ vs. time in 2nd order (a) $N = 3$ and (b) $N = 5$ Sierpinski carpet obstacle patterns. The continuous black lines are the power-law fits to the numerical data with slopes n given by Eq. (3). The insets in (b) show the fluid front locations at the times corresponding to the black circles. (For interpretation of the references to colour in this figure legend, the reader is referred to the web version of this article.)

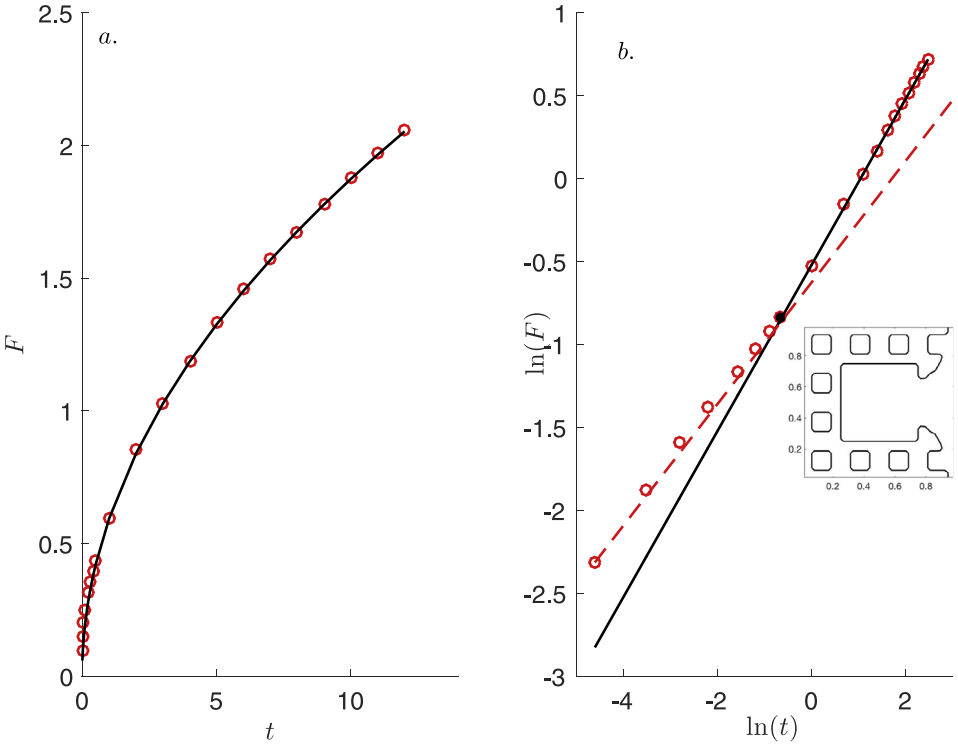

Fig. 3. Infiltration into a four fold repeat of a 2nd order $N = 4$, Sierpinski carpet. In panel *a.* it appears that the predicted infiltration $F(t)$ (red-circles) follows a normal diffusion power-law, $n = \frac{1}{2}$ (black-line). In the log-log plot in panel *b.*, however, we see that at early time the infiltration time exponent is sub-diffusive, the broken red line has a slope of $n = 0.366$. The insert in b. shows the fluid front in the vicinity of the transition back to normal diffusion (the black circle). (For interpretation of the references to colour in this figure legend, the reader is referred to the web version of this article.)

scaling in Eq. (3) (see Table 1). Only at later times, do we see the transition to normal diffusive behavior ($n = 0.5$).

3. Super-diffusive behavior

The scaling in Eq. (3) provides us with an independent means of arriving at the exponent n for single fractal carpets. All that is required is a calculation of the fractal dimension of the carpet and its borders, along with an estimate of the time exponent associated with the free diffusion of a particle. In the carpets we have tested so far, the fractal dimension of the border over which the infiltrating liquid enters the carpet is free of obstacles and hence has a fractal dimension of $D_B = 1$. It is straightforward though to create systems where the distribution of obstacles along the infiltrating boundary is fractal. For example, consider our $N = 3$ and $N = 5$ carpets shifted a half-phase to the right, see Fig. 4. In this case the flow obstacles along the infiltration boundary form a Cantor set with fractal dimension

$$D_B = \frac{\log(2)}{\log(N)} \tag{5}$$

By setting this new boundary, the scaling in Eq. (3) suggests power-law exponents $n > \frac{1}{2}$ (see Table 1), which would mean that for the exact same geometry the infiltration will now exhibit a super- as opposed to a sub-diffusive behavior. We confirm this by direct simulation on the $N = 3$ (Fig. 5*a.*) and $N = 5$ (Fig. 5*b.*) shifted carpets, where power-laws, using the appropriate calculated super-diffusion exponents in Table 1, provide a close match to observed values. This demonstrates that a domain with essentially the same heterogeneity structure can generate both sub- and super diffusive behavior. As a support for this finding, we point to a consistency with our results and observations of moisture infiltration into building materials. In particular, we note that the unshifted $N = 3$ carpet has a sub-diffusive exponent of $n = 0.424$, close to the experimental exponent $n_{exp} = 0.43$ reported by Gerolymatou et al. (2006), while the super-diffusive exponent $n = 0.599$, associated with the shifted $N = 3$ carpet, is close to the experimental exponent $n_{exp} = 0.58$ reported by Küntz and Lavallée (2001). Further, recognize, that in our analysis it is assumed that the advance of the fluid front within the carpet will be sub-diffusive ($\nu < \frac{1}{2}$). In some situations, however, the advance of the fluid front may not be sub-diffusive. For example, a recent neutron scattering study of water absorption in clay and silicate bricks shows fluid front evolution with exponents ν as high as 0.7 and 0.9 (El Abd, 2015). In these cases, the appearance of a super-diffusive infiltration is more likely but if on the infiltrating boundary $D_B = 1$ and the fractal dimension D_F of the domain is sufficiently small, sub-diffusive infiltration may still be observed.

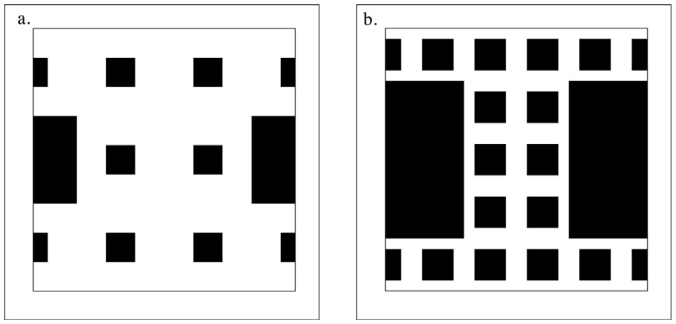

Fig. 4. Hele-Shaw obstacle patterns for a. the 2nd order $N = 3$ shifted Sierpinski carpet, and b. the 2nd order $N = 5$ shifted Sierpinski carpet.

Comparison of Figs. 1*a,b* and 4*a,b* helps to explain the apparently paradoxical feature of generating sub- and super- diffusion form the same heterogeneity structure. When infiltration begins at a border of dimension 1 (Fig. 1*a,b*), the front encounters a higher degree of disorder as it enters the carpet, with continuously decreasing available (open) length in the vertical (y) direction. Thus, the front penetration slows down as compared to a free medium, which explains the sub-diffusive scaling. On the other hand, when the infiltration begins at a fractal border (Fig. 4*a,b*), as the front moves, it encounters a continuously increasing available length. The front penetration is consequently faster in comparison with the normal diffusive scaling seen in a medium with homogeneously distributed obstacles; this explains the appearance of super-diffusive scaling.

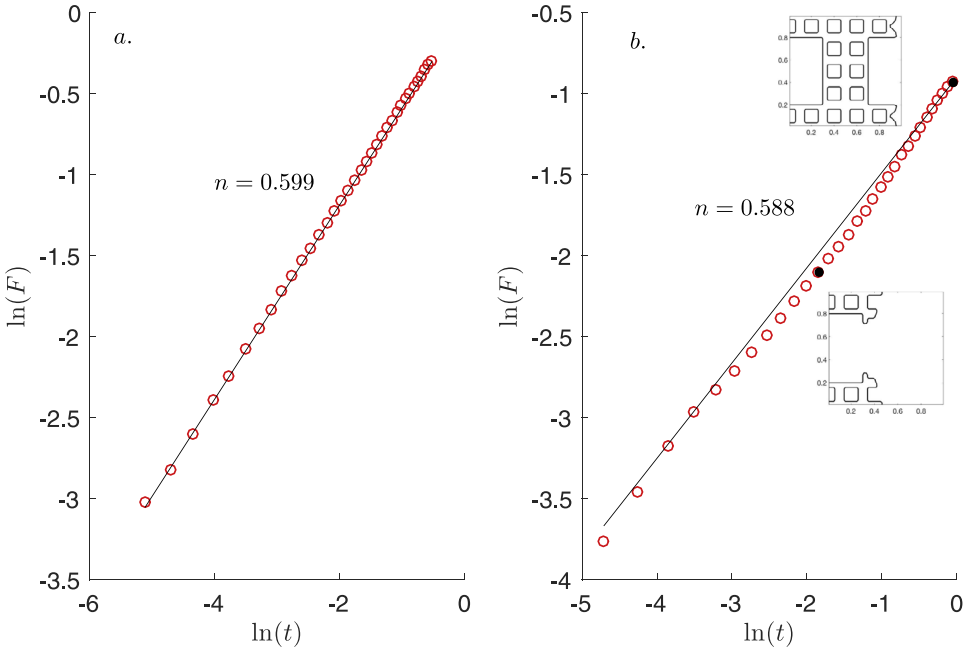

Fig. 5. Super-diffusive predictions for infiltration $F(t)$ (red-circles) into shifted obstacle patterns, *a.* $N = 3$ and *b.* $N = 5$. Predictions are compared with the power-law fits (black-lines) using the time exponent n from the scaling analysis in Eq. (3).The insets in (b) show the fluid front locations corresponding to the black circles. (For interpretation of the references to colour in this figure legend, the reader is referred to the web version of this article.)

Observation that the same form of heterogeneity can induce both sub- or super- diffusion has strong practical implications. Many argue that it would be ideal to be able to predict anomalous behaviors and transport parameters knowing only some structural details of a heterogeneous porous medium. Yet, the results here suggest that merely having a geostatistical representation of the heterogeneity of the system may not provide sufficient information to predict anything about the nature of anomalous behaviors one might expect. Rather, knowing details of the distribution of heterogeneity relative to the boundary is also essential.

4. Transitions from anomalous to normal behavior

To close we return to the previous result for infiltration into a carpet with a repeating pattern, Fig. 1c. Here we explore the nature of the transition from anomalous to normal diffusion. Our hypothesis, based on previous understanding of solute transport in heterogeneous porous media (e.g. Bolster et al., 2011; Dentz et al., 2004; Sund et al., 2016), is at that at very early times the infiltration will be Fickian ($n = 0.5$), then as the liquid encounters the first (smallest) obstacle this will switch to anomalous, and once the liquid has sampled all of the obstacle length scales a Fickian scaling will be reestablished. To test this, we define two *transition points*. We obtain the first $[t_1, F_1]$ by using the known analytical relationship, $F = \sqrt{2t}$, that holds in the initial obstacle free region. We arrive at the second $[t_2, F_2]$ by recording the time and infiltration length values at the point where half of the numerical cells in the last column of the first carpet ($x = 1$) are filled with liquid, i.e., $\sum_{i=1}^{n_{cell}} f_{i,j} > n_{cell}/2$, where n_{cell} is the number of cells in the column and $0 \le f_{i,j} \le 1$ is the value of the *liquid fraction* in cell (i, j). Our idea is that this condition coincides with the time when a representative vertical (oriented in the y direction) *averaged filling front* $x_M(t)$ passes from the first to the second carpet. On study of the *actual* filling front (Fig. 6) at this point, we note that the lagging part of the infiltration liquid is just clearing the largest obstacle ($x = 0.75$) while the leading liquid has entered the second carpet ($x > 1$); thus we consider this situation to be a sound indication that the infiltrating liquid has sampled all of the heterogeneity length scales present in the system.

In the simulation of the infiltration into this carpet sequence, in order to capture the very early time behavior, we use a variable time step, starting with the value $\Delta t_0 = 5 \times 10^{-5}$ and increasing the value by 10% between each time step until we reach the fixed maximum value

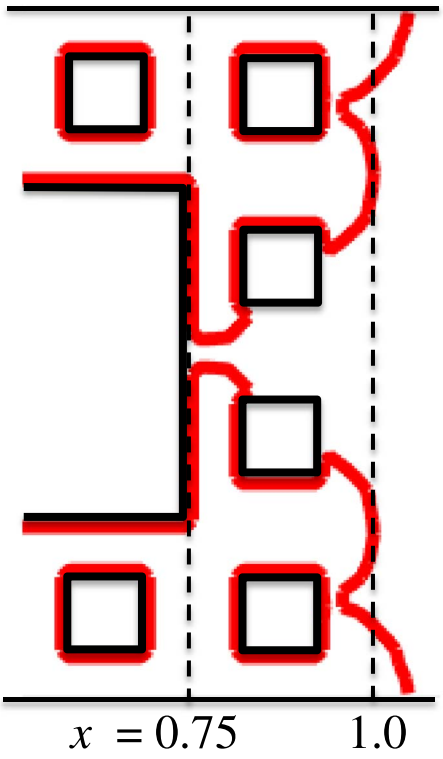

Fig. 6. Actual filing front (red-line) location at point in infiltration simulation where the representative vertical filling front, $x_M(t) = 1$, is located at the boundary between the first and second carpets. (For interpretation of the references to colour in this figure legend, the reader is referred to the web version of this article.)

$\Delta t_{\max} = 0.5$; the space step used is $\Delta x = \Delta y = \frac{1}{n_{cell}}$, $n_{cell} = 48$. Following the simulation, we fit two power laws with slopes $n = 0.5$ through each of our transition points and join these two points with a third power-law (see black lines in Fig. 7). Observation shows that these power-law fits pass through the simulation data (see red-circles) and reveal clear transitions (*knees*) in the transport exponents, with an early and late time Fickian diffusion behavior and an intermediate sub-diffusion behavior when the infiltrating liquid is sampling all the possible

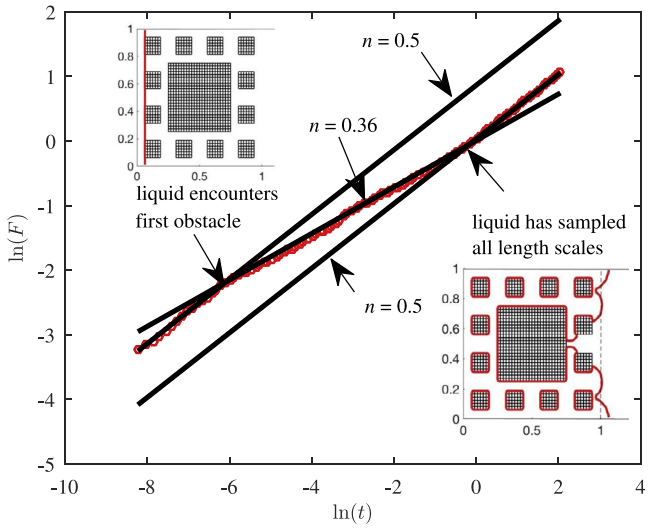

Fig. 7. Transitions between normal and sub- diffusive infiltration behavior in a three-fold repeat of a 2nd order, $N = 4$ carpet. The infiltration simulation predictions are shown as red circles. Black lines are linear fits in three scaling regions with the indicated slopes. (For interpretation of the references to colour in this figure legend, the reader is referred to the web version of this article.)

heterogeneity length scales located within the first fractal carpet. Moreover, the exponent of the fit in the intermediate region, $n = 0.360$, closely matches the exponent predicted with the random walk simulation scaling, $n = 0.366$, proposed by Aarão Reis (2016); see Eq. (3) and Table 1.

5. Explanation of the anomalous to normal transition

An interesting feature stands out in Fig. 7, namely the relatively rapid nature of the transitions in scaling, which appear to occur sharply as the fluid encounters the first obstacle and exits the first carpet respectively. Here we explore these transitions in more detail.

To start, we note that the first transition is a finite size effect, which is revealed because of the low $m = 2$ order of the carpet used in our simulation. This we feel is a reasonable mimic of what might be observed in a field setting but recognize that the signal of the initial normal behavior would be quickly quenched when the order of the fractal patten is increased. To illustrate, in a mth order N carpet, if we normalize the time to infiltrate the first carpet as $t = 1$, the time for the liquid to reach the first obstacle is N^{-2m}; as the order m increases it is easy to see how this time rapidly becomes negligible.

Our particular focus will be on the second transition in Fig. 7, i.e., the transition from anomalous back to normal diffusion; this transition will always manifest regardless of the order of the fractal carpet. In some ways this transition behavior is reminiscent of Taylor dispersion (e.g. Bolster et al., 2011; Sund et al., 2016; Taylor, 1954; Whitaker, 2013); i.e. the scaling of the second centered moment of a solute plume will scale in a Fickian manner after a time scale τ where the solute has had sufficient time to sample all of the heterogeneity in the system by diffusion ($\tau \sim L^2/D$, where L is a characteristic length scale and D is the diffusion coefficient). However there are two important differences: first the extremely sharp transition between the regimes here stands out in contrast to somewhat smoother transitions in transport systems and second, the transition is entirely determined by the structure of the heterogeneity and how long it takes for the applied pressure head to drive the front through the structure. Essentially there is no equivalent stochastic process like diffusion that causes the sampling and potentially different rates of sampling of the heterogeneity, rather due to the pseudo steady state, as the fluid advances to a new point in the domain, the full effect of the pressure head at the infiltrating boundary is instantaneously communicated. As such, in the case of a solute, the combination of heterogeneity structure and the strength of diffusion dictates the type and persistence of anomalous transport, while here it is the structure alone that dictates the behavior. By considering a simplified treatment of the infiltration into a fractal obstacle field we can provide a somewhat mechanistic explanation for this behavior.

Let us set the dimensions of each of the carpets as 1×1 and denote its porosity by μ. Also let us assume that we can characterize the infiltration into our sequence of 4 ($j = 1, 2, 3, 4$) carpets by considering that, at any point in time, the averaged position of the liquid infiltration can be represented as a vertical front, $x_M(t)$, aligned with the y-axis and normal to the prevailing x-directed flow. Then, drawing on a result in Voller (2015) (and consistently with the scaling approach in the appendix), we can show that the infiltration length into any given carpet element in the sequence is given as $F_{carpet} = \mu s^{\alpha}$, $\alpha = D_F - 1$, where $s = x_M - (j-1)$ is the position of the averaged filling front relative to the left hand edge of the carpet in question. In this way, when the filling front is in the j^{th} carpet, the infiltration length for the sequence as a whole is given by

$$F = \mu[(j-1) + (x_M - (j-1))^{\alpha}] \tag{6}$$

From this expression we notice that, in the first carpet ($j = 1$), the infiltration length has a power-law relationship with the liquid front position. In an average sense, however, we also note that F is constrained to increase in a linear fashion with x_M, i.e., at integer values of $x_M = j(=1, 2, 3. .)$, $F = j\mu$. Further, since for our carpets with pattern numbers $N = 3$, 4 or 5, the values of $0.7 \le \alpha \le 1$, once we move beyond $x_M = 1$, we will only see small and decreasing deviations from a linear relationship between F and x_M. Thus, as our averaged filling front moves out of the first carpet there is a strong tendency for changes in the infiltration length to become linear with front position, i.e., *when infiltration moves beyond the first carpet the diffusion nature of F is determined by the diffusion nature of x_M.*

To move forward let us examine how the diffusion nature of x_M changes with advance through the carpet sequence. On noting that the pressure head along $x = 0$ is $h = 1$ and assigning the pressure head along the liquid front to be gauge $h_{x_M} = 0$, we can assume that the speed of the front at a given time will be determined by the product of an *effective conductivity* $K(x_M)$ and the average head gradient between $x = 0$ and the front. On appropriate scaling in time,

$$\frac{dx_M}{dt} = \frac{\nu K(x_M)}{x_M}, \tag{7}$$

The material in our appendix tells us that, in the first carpet, $x_M \sim t^{\nu}$. This implies, from Eq. (7), that the representative conductivity in the first carpet scales as $K_1(x_M) \sim x_M^{\frac{2\nu-1}{\nu}}$. From this we can infer that in any carpet in our sequence ($j = 1, 2, 3, 4$) the representative conductivity in $(j-1) \le x \le (j-1) + s$ is $K_j(s) \sim s^{\frac{2\nu-1}{\nu}}$, where $0 \le s = x_M - (j-1) \le 1$ is length of liquid penetration into the carpet j. On the other hand, the representative conductivity in the *entire* liquid domain to that point, $0 \le x \le x_M$ needs to be evaluated by the harmonic mean

$$K(x_M) \sim \left[\frac{\frac{j-1}{x_M}}{K_{j-1}} + \frac{\frac{s}{x_M}}{s^{\frac{2\nu-1}{\nu}}}\right]^{-1} = \frac{j-1+s}{j-1+s^{\frac{1-\nu}{\nu}}}, \tag{8}$$

note, by the choice of our dimensions, that the representative conductivity for each fully filled carpet is $K_{j-1} = 1$. On recognizing that typical values of $\nu \sim 0.45 - 0.5$, we can conclude that in and beyond the second carpet, $j > 1$, the value of the representative conductivity Eq. (8) takes on a nearly constant value close to 1. As a result, in this region, the solution of Eq. (7) is

$$x_M = [2\nu t + (1 - 2\nu)]^{\frac{1}{2}}, \quad x_M \ge 1 \tag{9}$$

where the correction term $(1 - 2\nu)$ arises due to the initial condition at the end of the first carpet, i.e., $t = 1$ when $x_M = 1$. Since, as already

noted, we expect that $\nu \sim 0.45 - 0.5$ this correction will be small and we see that in and beyond the second carpet the average front movement has a close to normal behavior $x_M \sim t^{\frac{1}{2}}$. Thus, due to the fact that beyond the first carpet the infiltration F scales with the average front position x_M, we should expect that the infiltration will revert to a close to normal diffusive time scaling once our averaged filling front enters the second carpet.

The key driver in this reversion to normal diffusion is embodied in the nature of the averaging conductivity $K(x_M)$, see Eq. (8). At early infiltration times, when the liquid front is in the first carpet, the length scale over which the averaging is made is small and infiltrating liquid encounters changes in the heterogeneity (obstacle size) that have a large influence in determining the value of K. Here we see a power-law dependence in K on x_M and, through solution of Eq. (7), a sub-diffusive power-law dependence of x_M in time is maintained. This reflects the fact that as the liquid infiltrated into the first carpet it continues to encounter further non-explored heterogeneity structures that are sufficient to keep ahead of the "quenching" effect of an increasing averaging length scale. But once the infiltrating fluid has sampled all of the heterogeneity length scales, the earlier power-law exponent cannot "keep up" with the averaging length scale. From this point on, while we still see fluctuations in the value $K(x_M)$, they are around the constant value $K \sim 1$ and their amplitude rapidly decays with advance of x_M. So this simple description provides a mechanism to explain how a transition from anomalous to close to normal transport will rapidly occur once all of the heterogeneity length scales in the system have been sampled.

6. Robustness of the results

Here it has been useful to study infiltration into fractal obstacle fields for three reasons: (1) we have a validated direct numerical simulation, (2) predictions from the simulation provide a clear signal of anomalous transport behavior, and (3) the time exponent of this signal can be explained by the scaling associated with Brownian motion in fractal obstacle fields. To have practical benefit, however, it is worthwhile to discuss how the infiltration into our Hele-Shaw analog is related to more realistic porous media flows. First we note that the flow in a Hele-Shaw cell is a potential flow and thus the fluid flux is directly analogous to a Darcy flux in a porous medium. Indeed in the Hele-Shaw infiltration experiments reported in Filipovitch et al. (2016) it is argued, through scaling, that the set up matches the infiltration of water into a background media of gravel/sand containing impermeable flow obstacles. In a physical setting, however, we would expect much less abrupt changes in the fluidic conductivity. Thus, one way to model what might happen in a more realistic porous medium is to relax the sharp contrast between the channels and obstacles in our Hele-Shaw infiltration simulation. We do this by simulating infiltration into an $N = 3$ order $= 2$ cell ($\Delta x = \frac{1}{36}$, $\Delta t = 0.005$), assigning, to each computational cell in a channel, a fluidic conductivity chosen at random from the range [0.5, 1.5] and to each cell in an obstacle a random value from the range [0.0, 0.5]. In this way, our obstacles become permeable and the boundaries between channels and obstacles becomes fuzzy (see insets in Fig. 8). The simulations for this case still recover a strong power-law behavior and clearly show the switch from sub-to super-diffusion as the placement, of the now fuzzy obstacles, is shifted. Thus, this simulation indicates that, in studying infiltration into more realistic porous media, we should expect to see the anomalous behaviors observed in our Hele-Shaw simulations. Of course, as reflected in many of the papers we have cited here, a keen area of anomalous transport research is directed at understanding transport of solute phases in saturated porous media. In these situations it is possible that the exact behaviors associated with infiltration may manifest in a different fashion. However, since the underlying governing equations in both infiltration and solute transport in porous media share a common root (i.e., the Darcy equation) we do expect to see similar behaviors, that is, a switch

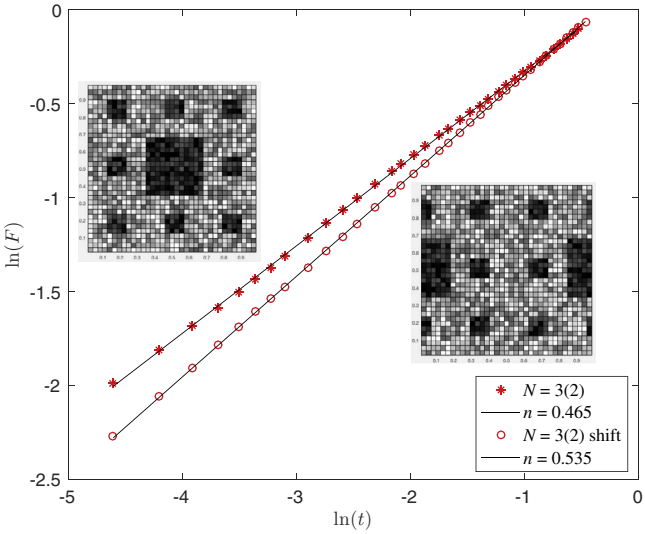

Fig. 8. Infiltration into porous domains that randomly distributed fluidic conductivity values over two ranges. Using an $N = 3$ order (2) carpet pattern as a base, the channels have values in the range [0.5, 1.5] and the obstacles in the range [0.0, 0.5]. The insets indicate the distribution based on a normal and shifted pattern.

between sub and super diffusion depending on the nature of the injection boundary and transition to normal transport once all heterogeneity sizes have been sampled.

There is no doubt that the simulations presented here and previous numerical and experimental work (Filipovitch et al., 2016; Voller, 2015) reveal that infiltration into fractal carpet objects, even with low order truncations, is power-law in time, with a sub-diffusive exponent. What is surprising, as noted originally in Voller (2015), is the fact that the exponent predicted for a particular carpet design does not have a notable dependence on the order of the fractal truncation. Although this has been fully investigated elsewhere (Filipovitch et al., 2016; Voller, 2015), for completeness it is given a brief exploration here. To this end, Fig. 9 shows the log-log infiltration predictions for an N = 3 carpets with orders 2, 3 and 4; the best-fit slopes through these predictions is extremely consistent, $n = 0.422$, $n = 0.421$, and $n = 0.421$ respectively and close to the fractal theoretical value of $n = 0.424$ (see Table 1). Thus, we conclude, that to obtain anomalous diffusion for infiltration, it is not necessary to have a high order fractal distribution of heterogeneity; rather 2–3 heterogeneity scales (with the largest approaching the domain size) is sufficient.

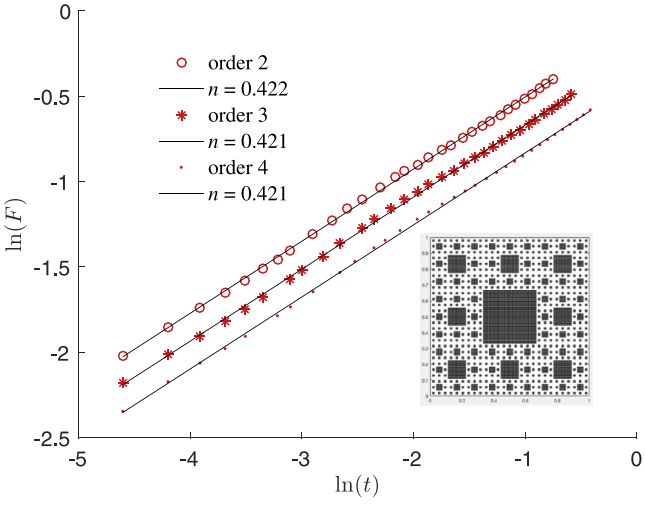

Fig. 9. Infiltration into an $N = 3$ obstacle pattern with truncation order of 2, 3 and 4. The inset shows the obstacle pattern for the $N = 3$ order 4 carpet.

7. Conclusion

In brief summary, the basic component in our infiltration simulations is a horizontally ($x - y$ plain) oriented Hele-Shaw cell containing a fractal pattern (Sierpinski carpet) of flow obstacles. The direction of flow is principally in the x direction and liquid is infiltrated into an initially gas filled domain by imposing and holding a fixed gauge pressure along the y boundary at $x = 0$.

We have shown that when our domain consists of a single carpet, aligned so that the boundary over which the infiltrating liquid enters is free of flow obstacles, the evolution of the infiltration length exhibits a sub-diffusive behavior. On the other hand, when the infiltrating boundary contains obstacles distributed as a fractal (a Cantor set)—-simply obtained by shifting the *same* obstacle carpet as before a $\frac{1}{2}$ phase in the longitudinal direction—the infiltration is super-diffusive. Both the sub- and super- behaviors can be explained by an appropriate scaling analysis.

In addition we have examined infiltration into a domain consisting of a repeating sequence of fractal carpet components. Here we show that, once the infiltrating flow has sampled the largest heterogeneity length scale in the system (i.e., as the infiltrating flow moves from the first to the second component) the progress of the infiltration undergoes a rapid transition from an anomalous to a normal diffusive like scaling.

The Hele-Shaw cell set up used in our simulations, which have been extensively validated with experimental measurements, is physically equivalent to horizontal fluid infiltration into a gravel/sand porous medium containing a distribution of flow obstacles of varying sizes. Thus our findings have direct consequences for porous media. In particular our results explain why it would be possible, simply by the nature of the boundary over which flow enters, to observe both sub- and super transport behaviors in a given medium without fundamentally changing the nature of the heterogeneity distribution within the medium itself. Our results also clearly illustrate and explain why, once the length scale of the domain of interest exceeds the length scale of the largest heterogeneity in the system, signals of anomalous behavior are rapidly quenched and normal scaling begins.

Acknowledgments

VRV acknowledge support from the National Science Foundation through Grant EAR-1318593, Generalized Transport Models in Earth Surface Dynamics. FDAAR was partially supported by an MTS visiting professorship, provided by the Department of Civil, Environmental, and Geo- Engineering, University of Minnesota, and by Brazilian agencies CNPq (304766/2014-3) and Faperj (E-26/202941/2015). We also appreciate significant discussion with colleagues Kimberly Hill, Mark Meerschaert, and Chris Paola. In addition we acknowledge the insight and suggestions provided by the reviewers.

Appendix A. Appendix: Scaling approach

Here we outline the arguments for adopting the scaling approach which relates the length of infiltration to the exponent $\nu < 1/2$ associated with the spreading of a free random walker within a fractal obstacle pattern.

First to provide some background we discuss key features of the direct simulation for infiltration into a Hele-Shaw cell. As outlined in Voller (2015) the governing equation is the volume of fluid equation

$$\frac{\partial f}{\partial t} = \nabla(K\nabla h) \tag{A.1}$$

where $0 \le f \le 1$ is a fill factor, and h is the pressure head. The initial condition is $f = 0$ and the boundary conditions are a fixed head $h = 1$ along $x = 0$, a fixed head $h = 0$ along $x = 1$ and no flow conditions along $y = 0$ and $y = 1$. To make a connection between the fill factor and head the additional constitutive relationship $h = 0$ at all points where $f < 1$ is used in the numerical solution . The subsequent simulation (see details in Voller (2015)) is based on a mesh ($n_{cell} \times n_{cell}$) of uniform sized, node centered, control volumes. The main dependent variables stored at a node point (i, j) is the pressure head $h_{i,j}$ and the fill fraction, $f_{i,j}$. This latter variable takes values of $f_{i,j} = 1$ in control volumes that are filled with liquid, $f_{i,j} = 0$ in control volumes that are empty (gas filled), and $0 < f_{i,j} < 1$ at the liquid /gas front. Note, as detailed in Voller (2015), the numerical solution in the simulation is constructed so that the liquid only has a width of one control volume and that, in control volumes where $f_{i,j} < 1$, the associated pressure head takes the value $h_{i,j} = 0$.

From the numerically calculated nodal fill fraction field we can make two separate measures for the advance of infiltration with time. The first is the advance $x_M(t)$ of an averaged liquid front that is aligned in the y-direction. In our work here, motivated by the fundamental connection between the diffusion and random walk processes, we have made the *ansatz* that the time exponent associated with this representative filling front matches the exponent ν observed in the spreading of random walkers starting from a common point within the fractal carpet (see 4th column of Table 1), i.e, $x_M \sim t^{\nu}$.

The other measure of infiltration, as used in the body of the paper, is the infiltration length $F(t) = {n_{cell}}^2 \sum f_{i,j}$, i.e., [*the plan-view area containing the liquid /the length of the boundary over which the infiltrating liquid enters the domain*]. In this way we can envisage a representative infiltration process in an N pattern carpet of order $m \ge 1$ where at each stage $p = 1, 2, 3. .m$, to maintain similarity, the expanding infiltrated domain fits into a box of size $x_M \times x_M$, with $x_M = N^p$ length units, i.e., a domain that covers the p^{th} order of the chosen carpet. To move forward, we note that the fraction of open area in this domain (the porosity) is given by $\mu = \left[\frac{4N-4}{N^2}\right]^p$. Assuming a Cantor set distribution of obstacles for the carpets shifted a half phase to the right (Fig. 4), the fraction of open length on the infiltrating boundary is $\mu_B = \left[\frac{2}{N}\right]^p$. Thus, according to the given definition, the infiltration length can be expressed as

$$F = \frac{\mu N^p N^p}{\mu_B N^p} \tag{A.2}$$

From here, with appropriate algebra, it can be shown that $F \sim x_M^{D_F - D_B}$. On substitution of the power-law for the advance of the representative liquid front $x_M \sim t^{\nu}$, the scaling relation in Eq. (3) immediately follows.

References

Aarão Reis, F.D.A., 2016. Scaling relations in the diffusive infiltration in fractals. Phys. Rev. E 94, 052124. http://dx.doi.org/10.1103/PhysRevE.94.052124.

Akkermans, E., Benichou, O., Dunne, G.V., Teplyaev, A., Voituriez, R., 2008. Spatial log-periodic oscillations of first-passage observables in fractals. Phys. Rev. E 86, 061125.

Aubeneau, A.F., Hanrahan, B., Bolster, D., Tank, J.L., 2014. Substrate size and

heterogeneity control anomalous transport in small streams. Geophys. Res. Lett. 41 (23), 8335–8341.
Aubeneau, A.F., Martin, R.L., Bolster, D., Schumer, R., Jerolmack, D., Packman, A., 2015. Fractal patterns in riverbed morphology produce fractal scaling of water storage times. Geophys. Res. Lett. 42 (13), 5309–5315.
Bab, M.A., Fabricius, G., Albano, E.V., 2008a. On the occurrence of oscillatory modulations in the power law behavior of dynamic and kinetic processes in fractals. EPL 81, 10003.
Bab, M.A., Fabricius, G., Albano, E.V., 2008b. Revisiting random walks in fractal media: on the occurrence of time discrete scale invariance. J. Chem. Phys. 128, 044911.
Balankin, A.S., 2017. The topological Hausdorff dimension and transport properties of Sierpiński carpets. Phys. Lett. A 381 (34), 2801–2808.
Batchelor, G.K., 1967. An Introduction to Fluid Dynamics. Cambridge University Press, Cambridge, UK.
Benson, D.A., Schumer, R., Meerschaert, M.M., Wheatcraft, S.W., 2001. Fractional dispersion, Lévy motion, and the made tracer tests. Dispersion in Heterogeneous Geological Formations. Springer, pp. 211–240.
Berkowitz, B., Cortis, A., Dentz, M., Scher, H., 2006. Modeling non-Fickian transport in geological formations as a continuous time random walk. Rev. Geophys. 44, RG2003. http://dx.doi.org/10.1029/2005RG000178.
Berkowitz, B., Scher, H., 1997. Anomalous transport in random fracture networks. Phys. Rev. Lett. 79 (20), 4038–4041.
Bijeljic, B., Blunt, M.J., 2006. Pore-scale modeling and continuous random walk analysis of dispersion in porous media. Water Resour. Res. 42, W01202. http://dx.doi.org/10.1029/2005WR004578.
Bolster, D., Valdés-Parada, F.J., Le Borgne, T., Dentz, M., Carrera, J., 2011. Mixing in confined stratified aquifers. J. Contam. Hydrol. 120, 198–212.
Bruschke, M.V., Advani, S.G., 1990. A finite-element control volume approach to mold filling in anisotropic porous-media. Polym. Compos. 11, 398–405.
Cushman-Roisin, B., 2008. Beyond eddy diffusivity: an alternative model for turbulent dispersion. Environ. Fluid Mech. 8 (5–6), 543–549.
De Anna, P., Le Borgne, T., Dentz, M., Tartakovsky, A.M., Bolster, D., Davy, P., 2013. Flow intermittency, dispersion, and correlated continuous time random walks in porous media. Phys. Rev. Lett. 110 (18), 184502.
Dentz, M., Bolster, D., 2010. Distribution-versus correlation-induced anomalous transport in quenched random velocity fields. Phys. Rev. Lett. 105 (24), 244301.
Dentz, M., Cortis, A., Scher, H., Berkowitz, B., 2004. Time behavior of solute transport in heterogeneous media: transition form anomalous to normal transport. Adv. Water Resour. 27, 155–173.
Edery, Y., Guadagnini, A., Scher, H., Berkowitz, B., 2014. Origins of anomalous transport in heterogeneous media: structural and dynamic controls. Water Resour. Res. 50, 1490–1505. http://dx.doi.org/10.1002/2013WR015111.
Einstein, A., 1905. Über die von der molekularkinetischen theorie der tärme geforderte bewegung von in ruhenden flüssigkeiten suspendierten feilchen, (on the motion of small particles suspended in a stationary liquid, as required by the molecular kinetic theory of heat). Annalen der Physik 17, 549–560.
El Abd, A., 2015. A method for moisture measurement in porous media based on epithermal neutron scattering. Appl. Radiat. Isot. 105, 150–157.
Eliazar, I., Klafter, J., 2011. Anomalous is ubiquitous. Ann. Phys. 326 (9), 2517–2531.
Falcini, F., Foufoula-Georgiou, E., Ganti, V., Paola, C., Voller, V.R., 2013. A combined nonlinear and nonlocal model for topographic evolution in channelized depositional systems. J. Geophys. Res. 118, 1617–1627. http://dx.doi.org/10.1002/jgrf.20108.
Filipovitch, N., Hill, K.M., Longjas, A., Voller, V.R., 2016. Infiltration experiments demonstrate an explicit connection between heterogeneity and anomalous diffusion behavior. Water Resour. Res. 52, 5167–5178. http://dx.doi.org/10.1002/2016WR018667.
Finnegan, N.J., Schumer, R., Finnegan, S., 2014. A signature of transience in bedrock river incision rates over timescales of 10^4 –10^7 years. Nature 505, 391–394.
Foufoula-Georgiou, E., Ganti, V., Dietrich, W.E., 2010. A nonlocal theory of sediment transport on hillslopes. J. Geophys. Res. 115, F00A16. http://dx.doi.org/10.1029/2009JF001280.
Ganti, V., Meerschaert, M.M., Foufoula-Georgiou, E., Viparelli, E., Parker, G., 2010. Normal and anomalous diffusion of gravel tracer particles in rivers. J. Geophys. Res. 115, F00A12.
Gerolymatou, E., Vardoulakis, I., Hilfer, R., 2006. Modelling infiltration by means of a non-linear fractional diffusion model. J. Phys. D 39, 4104–4110.
González, C., Richter, D.H., Bolster, D., Bateman, S., Calantoni, J., Escauriaza, C., 2017. Characterization of bedload intermittency near the threshold of motion using a Lagrangian sediment transport model. Environ. Fluid Mech. 17 (1), 111–137.
Gooseff, M.N., LaNier, J., Haggerty, R., Kokkeler, K., 2005. Determining in-channel (dead zone) transient storage by comparing solute transport in a bedrock channel–alluvial channel sequence, oregon. Water Resour. Res. 41 (6), W06014.
Gouze, P., Le Borgne, T., Leprovost, R., Lods, G., Poidras, T., Pezard, P., 2008. Non-Fickain dispersion in porous media: 1. multiscale measurements using single-well injection withdrawal tracer tests. Water Resour. Res. 44, W06426. http://dx.doi.org/10.1029/2007WR006278.
Haggerty, R., Wondzell, S.M., Johnson, M.A., 2002. Power-law residence time distribution in the hyporheic zone of a 2nd-order mountain stream. Geophys. Res. Lett. 29 (13), 18-1–18-4.
Havlin, H., Ben-Avraham, D., 2002. Diffusion in disordered media. Adv. Phys. 51, 187–292.
Hirt, C.W., Nichols, B.D., 1981. Volume-of fluid (vof) method for the dynamics of free boundaries. J. Comput. Phys. 39, 201–225.
Kang, P.K., Brown, S., Juanes, R., 2016. Emergence of anomalous transport in stressed rough fractures. Earth Planet. Sci. Lett. 454, 46–54.
Kang, P.K., de Anna, P., Nunes, J.P., Bijeljic, B., Blunt, M.J., Juanes, R., 2014. Pore-scale intermittent velocity structure underpinning anomalous transport through 3-d porous media. Geophys. Res. Lett. 41, 6184–6190. http://dx.doi.org/10.1002/2014GL061475.
Kim, M.H., Yoon, D.H., Kim, I., 1993. Lower and upper bounds for the anomalous diffusion exponent on Sierpinski carpets. J. Phys. A 26 (21), 5655–5660.
Küntz, M., Lavallée, P., 2001. Experimental evidence and theoretical analysis of anomalous diffusion during water infiltration in porous building materials. J. Phys. D 34, 2547–2554.
Le Borgne, T., Dentz, M., Carrera, J., 2008. Lagrangian statistical model for transport in highly heterogeneous velocity fields. Phys. Rev. Lett. 101 (9), 090601.
Le Borgne, T., Gouze, P., 2008. Non-Fickain dispersion in porous media: 2. model validation from measurements at different scales. Water Resour. Res. 44, W06427. http://dx.doi.org/10.1029/2007WR006279.
Neuman, S.P., Tartakovsky, D.M., 2009. Perspective on theories of non-Fickian transport in heterogeneous media. Adv. Water Resour. 32, 670–680.
Reis, F.D.A.A., 1995. Finite-size scaling for random walks on fractals. J. Phys. A 28 (22). 6277–5287
Schumer, R., Meerschaert, M.M., Baeumer, B., 2009. Fractional advection-dispersion equations for modeling transport at the earth surface. J. Geophys. Res. 114, F00A07. http://dx.doi.org/10.1029/2008JF001246.
Serrano, S.E., 1997. Non-Fickian transport in heterogeneous saturated porous media. J. Eng. Mech 123, 70–76.
Seymour, J.D., Gage, J.P., Codd, S.L., Gerlach, R., 2004. Anomalous fluid transport in porous media induced by biofilm growth. Phys. Rev. Lett. 93 (19), 198103.
Stark, C.P., Foufoula-Georgiou, E., Ganti, V., 2009. A nonlocal theory of sediment buffering and bedrock channel evolution. J. Geophys. Res. 114, F01029. http://dx.doi.org/10.1029/2008JF000981.
Sund, N.L., Bolster, D., Benson, D.A., 2016. Testing the limits of the spatial Markov model for upscaling transport: the role of nonmonotonic effective velocity autocorrelations. Phys. Rev. E 94 (4), 043107.
Taylor, G.I., 1954. Diffusion and mass transport in tubes. Proc. Phys. Soc. Sect. B 67 (12), 857.
Voller, V.R., 2011. On a fractional derivative form of the Green-Ampt infiltration model. Adv. Water Resour. 34, 257–262.
Voller, V.R., 2015. A direct simulation demonstrating the role of spacial heterogeneity in determining anomalous transport. Water Resour. Res. 51, 2119–2127. http://dx.doi.org/10.1002/2014WR016082.
Voller, V.R., Chen, Y.F., 1996. Prediction of filling times of porous cavities. Int. J. Numer. Methods Fluids 23, 661–672.
Voller, V.R., Ganti, V., Paola, C., Foufoula-Georgiou, E., 2012. Does the flow of information in a landscape have direction? Geophys. Res. Lett. 39, L01403. http://dx.doi.org/10.1029/2011GL050265.
Voller, V.R., Paola, C., 2010. Can anomalous diffusion describe depositional fluvial profiles? J. Geophys. Res. 115, F00A13. http://dx.doi.org/10.1029/2009JF001278.
Wang, L., Cardenas, M.B., 2014. Non-Fickian transport through two-dimensional rough fractures: assessment and prediction. Water Resour. Res. 39, 871–884. http://dx.doi.org/10.1002/2013WR014459.
Whitaker, S., 2013. The Method of Volume Averaging. 13 Springer Science & Business Mediahttp://dx.doi.org/10.1007/978-94-017-3389-2.